JACS
JOURNAL OF THE AMERICAN CHEMICAL SOCIETY
pubs.acs.org/JACS
Article

Multimodal Imaging Probe Development for Pancreatic β Cells: From Fluorescence to PET

Nam-Young Kang,△ Jung Yeol Lee,△ Sang Hee Lee, In Ho Song, Yong Hwa Hwang, Min Jun Kim, Wut Hmone Phue, Bikram Keshari Agrawalla, Si Yan Diana Wan, Janise Lalic, Sung-Jin Park, Jong-Jin Kim, Haw-Young Kwon, So Hee Im, Myung Ae Bae, Jin Hee Ahn, Chang Siang Lim, Adrian Kee Keong Teo, Sunyou Park, Sang Eun Kim, Byung Chul Lee, Dong Yun Lee,* and Young-Tae Chang*

Cite This: J. Am. Chem. Soc. 2020, 142, 3430−3439

ABSTRACT: Pancreatic β cells are responsible for insulin secretion and are important for glucose regulation in a healthy body and diabetic disease patient without prelabeling of islets. While the conventional biomarkers for diabetes have been glucose and insulin concentrations in the blood, the direct determination of the pancreatic β cell mass would provide critical information for the disease status and progression. By combining fluorination and diversity-oriented fluorescence library strategy, we have developed a multimodal pancreatic β cell probe **PiF** for both fluorescence and for PET (positron emission tomography). By simple tail vein injection, **PiF** stains pancreatic β cells specifically and allows intraoperative fluorescent imaging of pancreatic islets. **PiF**-injected pancreatic tissue even facilitated an antibody-free islet analysis within 2 h, dramatically accelerating the day-long histological procedure without any fixing and dehydration step. Not only islets in the pancreas but also the low background of **PiF** in the liver allowed us to monitor the intraportal transplanted islets, which is the first in vivo visualization of transplanted human islets without a prelabeling of the islets. Finally, we could replace the built-in fluorine atom in **PiF** with radioactive 18F and successfully demonstrate in situ PET imaging for pancreatic islets.

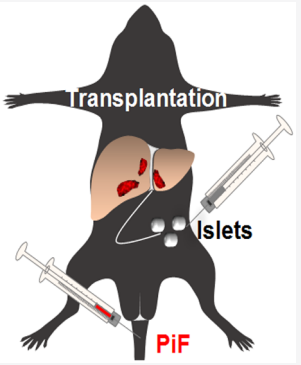

INTRODUCTION

Developing an advanced imaging technology for live pancreatic β cells has become of great interest over the past decade in the diabetes area.[1−3] Pancreatic β cells are responsible for insulin synthesis and secretion in response to hyperglycemia, and insulin controls the uptake of glucose from the blood into target organs such as fat or muscle. The dysregulation of insulin production, secretion, or its downstream signaling would disturb the proper control of the blood glucose concentration. A persistent high blood glucose level is a signature biomarker of diabetic diagnosis and prognosis. Type 1 diabetes (T1D) is caused by pancreatic β-cell death and consiquently a decrease in insulin production, giving rise to hyperglycemia as a result. Therefore, patients with T1D are expected to have reduced β-cell mass due to gradual β-cell destruction.[4] Type 2 diabetes (T2D) is more complicated. Through multiple chronic causes, the blood glucose concentration can rise, and the pancreatic β-cell mass is also increased initially to secrete more insulin for compensation. Hyperinsulinemia occurs in the presence of insulin resistance, and eventually β-cell death occurs.[3] Therefore, beyond measuring glucose and insulin concentrations in the blood, an ability to determine the pancreatic β-cell mass noninvasively at various time points would be revolutionary in monitoring the progression of diabetes and prognosis upon drug treatment. To determine the β-cell mass accurately, the currently possible way is a histological analysis of pancreatic specimens obtained from patients through an operation. However, this surgical process is invasive and thus difficult to use as a routine prognostic method and is able to estimate the β-cell mass only within a particular area, not for the whole pancreas, due to the uneven number and distribution of islets in the human pancreas.[4,5] Hence, a nonsurgical and noninvasive visualization method for the accurate measurement of the β-cell mass via a specific molecular probe is highly desired for the stratification of patients at diagnosis and follow up as the disease progresses.

Current imaging technologies provide different information in terms of penetration, resolution, and sensitivity along with anatomical, physiological, and cellular contexts. Chromogenic small-molecule probes such as Newport green[6] and dithiazone (DTZ)[7] have been used for the ex vivo imaging of pancreatic

Received: October 17, 2019
Published: February 10, 2020

https://dx.doi.org/10.1021/jacs.9b11173
J. Am. Chem. Soc. 2020, 142, 3430−3439

islets and for the facilitated islet isolation for transplantation therapy.

Advancements in clinical practice aim to develop a noninvasive imaging modality for pancreatic β cells based on the magnetic resonance imaging (MRI), positron emission tomography (PET), and single-photon emission computed tomography (SPECT) platforms. The advantages of MRI include the high spatial resolution, contrast, and penetration depth of soft organs. The ex vivo labeling of islets with fluorescently labeled nanoparticles[8] or encapsulation with MRI-detectable magnetocapsules[9] allows transplanted islets to be monitored under the kidney capsules or in the livers of recipients. However, a visualizing method of unlabeled endogenous islets using an MRI technique has not yet been demonstrated.

Applying PET imaging to pancreatic β-cell biomarkers is limited by the availability of specific radiotracers. As early as 2000, the most common PET imaging probe, ^{18}F-FDG (2-deoxy-2-^{18}F-fluoro-D-glucose), was used for imaging and quantifying the endocrine pancreas in rats.[10,11] While useful, the multiple binding sites of ^{18}F-FDG prompted a quest for more specific β-cell probes. Radiolabeled ^{18}F-fluoropropyl-dihydrotetrabenazine (^{18}F-FP-DTBZ) and its derivatives targeting vesicular monoamine transporter 2 (VMAT2) have been used for β-cell imaging. However, not all of the immunoreactivity from VMAT2 is associated with β cells.[11] In addition to VMAT2, various β-cell-specific imaging reagents were recently introduced, targeting new biomarkers such as sulfonylurea receptors (SUR-1), glucagon-like peptide 1 (GLP-1), free fatty acid receptor 1 (FFAR1), and β-cell-specific antigens.[12−14] Of them, Mn-DPDP,[15] ^{11}C-DTBZ,[16] ^{18}F-AV-133,[17] ^{18}F-FDOPA,[18] and ^{68}Ga-NOTA-exendin-4[19] are representative probes, which were tried in clinical setups and evaluated for β-cell mass with great promise.[20] Still, there is a missing link between fluorescent probe application and PET imaging of pancreatic β cells for the systematic comparison between ex vivo and in vivo imaging results.

We have worked on pancreatic α-[21] and β-cell-selective probe development for the past decade and published the first fluorescent small-molecule probe for β cells, **PiY** (pancreatic islet yellow).[22] Through tail vein injection, **PiY** demonstrated selective staining and facilitated the isolation of live islets from mice. While useful for the ex vivo application of islet imaging, **PiY** had a limitation in terms of a long tissue-handling procedure over 10 h. **PiY** also showed higher localization in the liver than in the pancreas through a pharmacokinetic study, thus hampering its applicability to the imaging of transplanted islets in the liver.

We envisioned that an ideal β-cell imaging probe is optically active (fluorescent), has low background in other organs, and eventually is convertible to a PET probe without chemical modification. On the basis of these criteria, we herein report a novel β-cell probe, **PiF** (pancreatic islet fluorinated probe), with a dual-modality application both for optical and PET imaging of the β-cell mass.

RESULTS

Identification of the Pancreas-Selective PiF Probe from DOFLA. The diversity-oriented fluorescence library approach (DOFLA) was developed in the Chang laboratory, and DOFL is composed of thousands of small fluorescent molecules in library formats.[23] Through DOFLA and combining DOFL with unbiased screening, various fluorescent sensors and imaging probes have been developed and demonstrated for different cells and tissues.[24,25] For this project, we started in vitro screening of DOFL to pick up candidates with an increase in fluorescence upon addition of insulin, assuming that the insulin sensor would be a potentially selective probe for β cells. From the primary screening, six hits were found from the rosamine library,[26] and the selected compounds (Figure S1A) were retested in a range of insulin concentrations, showing a fluorescence increase in a dose-dependent manner against insulin (Figure S1B). Using the molecular information from the six candidates, we shuffled the structure and also incorporated the fluorine atom, which can be subsequently replaced by the ^{18}F radioisotope for PET probe generation to yield three candidate molecules (Figure 1A). As expected, all three candidate molecules showed an excellent insulin response in a dose-dependent manner. As the main limitation of previously reported probe **PiY**[22] was an unfavorable organ distribution in animal tests, we subjected the three candidate molecules to an in situ pharmacokinetic study in mice. After tail vein injection (300 μM, 250 μL), the fluorescence signal of injected probes throughout abdominal organs including the kidney, pancreas, liver, spleen, and fat pad

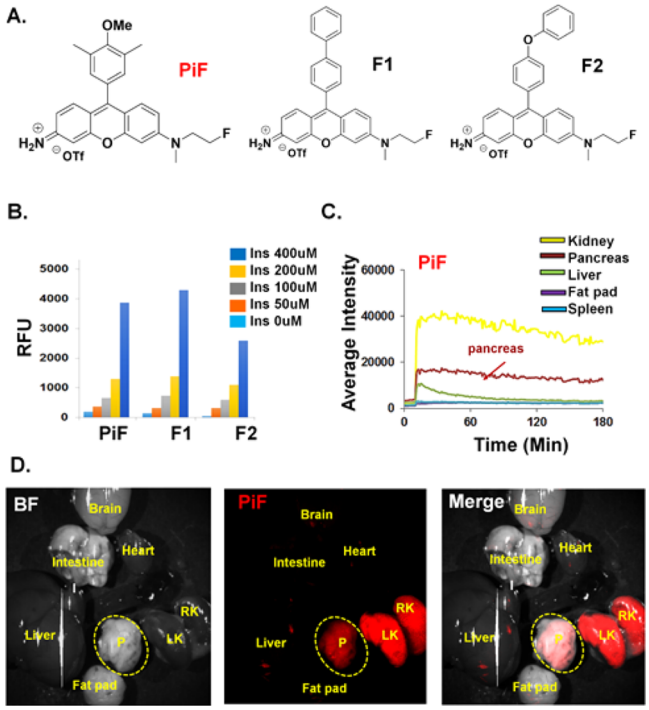

Figure 1. Development of pancreatic islet fluorinated probe **PiF**. (A) Chemical structures of **PiF** and derivatives of **PiF** (F1 and F2). (B) In vitro insulin responses of **PiF**, F1, and F2. Relative fluorescence units (RFUs) of **PiF**, F1, and F3 at 0.5 μM with different concentrations of bovine insulin in 20 mM HEPES buffer (1% DMSO, pH 7.4). (C) Fluorescence tissue distribution of **PiF**. The probe was dissolved in 2% BSA at 300 μM (3% DMSO) and injected intravenously (250 μL) after anesthesia. The fluorescence intensity is observed from different abdominal organs (kidney, pancreas, liver, fat pad, and spleen) during 3 h under a Texas red filter (ex, 540−580; em, 610 long pass). (D) Ex vivo fluorescent images of organs. (Left) Bright-field image of organs. (Middle) Fluorescent image of **PiF**. (Right) Merged images of BF and **PiF**. Yellow dot circles represent the pancreas samples. All images were taken using a Leica MZ10 customized modular stereo microscope for fluorescent imaging.

https://dx.doi.org/10.1021/jacs.9b11173
J. Am. Chem. Soc. 2020, 142, 3430−3439

was monitored for 3 h while the animal was under anesthesia. Compound **F2** showed a similar fluorescence intensity signal in both the liver and pancreas (Figure S2A), which is not desirable for whole-body imaging. The liver is anatomically close to and also much larger than the pancreas, and thus it would be difficult to isolate the two organ signals from the imaging data. Compound **F1** had a weaker fluorescence signal (over about half of the pancreas) in the liver but remained at significant levels over the 3 h (Figure S2B).

In contrast, **PiF** showed some signal in the liver in the beginning that was gradually reduced over time. One hour after injection, the fluorescence signal of **PiF** in the liver dropped down to almost the baseline level, while the sign-in pancreas remained significantly high (Figure 1C). Considering the half-life of ^{18}F to be 110 min, the signal profile of **PiF** seemed reasonable for a couple of hours of monitoring. After 3 h of supervision, the pancreas was harvested and observed under the fluorescence microscope, and **PiF** and F1 showed a good contrast for islets but F2 did not (data not shown). On the basis of these observations, we selected **PiF** as the best candidate for further development. It is noteworthy that all three compounds showed a stronger signal in the kidney than in the pancreas and the signal decreased over time, which may be due to the compounds' excretion process. After dissection, we evaluated the remaining fluorescence signal from several tissues, including the brain and heart by ex vivo imaging (Figure 1D). Both the kidney and pancreas manifested a higher fluorescence intensity than other tissues, which is consistent with the in situ biodistribution monitoring data. While the fluorescence signal of **PiF** in the kidney is stronger than in the pancreas, discrimination of the imaging signal is expected to be feasible due to the anatomical distance between the two organs. With **PiF**, we further investigated in vitro selectivity against albumin and glucagon, which are the most abundant proteins in the serum and hormone secreted from α cells, respectively. As expected, **PiF** responded strongly to insulin but much more weakly to albumin or glucagon (Figure S3). Therefore, **PiF** selectivity in β cells might be due to the selective binding to and the turn-on effect by insulin of high concentration in β cells. Through these procedures, we identified promising pancreatic β-cell probe **PiF** [(λ_{ex} = 535 nm, λ_{em} = 565 nm, quantum yield (Φ) = 0.51 in DMSO, extinction coefficient (ε) at 535 nm = 43 000 M^{-1} cm^{-1} in DMSO (Figure S4)] that allows chemical modification by introducing a radioactive ^{18}F into a PET tracer (Scheme 1).

Ex Vivo Visualization of Live and Healthy Pancreatic Islets with the PiF Probe. The conventional β-cell imaging procedure includes insulin or other relevant antibody-based immunohistochemistry, which is expensive and a labor-intensive, time-consuming procedure. Previously, we devised a protocol for measuring the β-cell mass using **PiY**, which does not require any antibody for immunostaining (Figure 2A, **PiY** protocol).[22] With this protocol, both **PiY** and **PiF** can be used to visualize pancreatic β cells of islets on the cryo-tissue sections (Figure 2B). While useful without the need for antibody, this method still requires paraformaldehyde fixing (2 h) and dehydration with 30% sucrose (usually at least 12 h). We further optimized the staining procedure with **PiF** and dramatically shortened the whole procedure from a day to a couple of hours by dropping the fixation and dehydration steps (Figure 2A **PiF** protocol). Using this improved protocol, staining with **PiF** worked well, but not with **PiY** (Figure 2C). We then tested this protocol with **PiF** in a type 1 diabetic

Scheme 1. Synthesis Scheme of PiF[a]

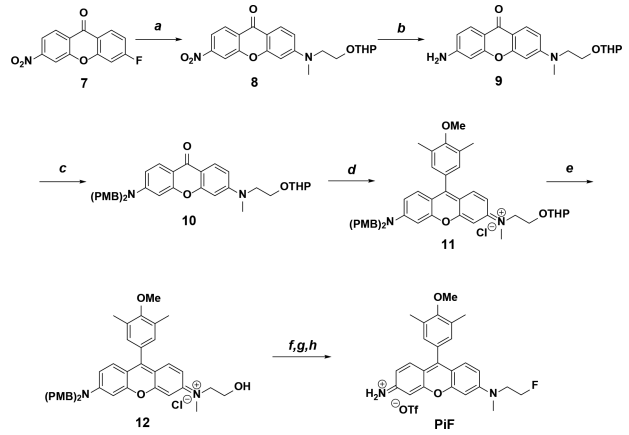

[a]Reagents and conditions: (a) *N*-methyl-2-(tetrahydro-2*H*-pyran-2-yloxy)ethanamine, DMSO, 90 °C, overnight, 37%; (b) 10% Pd/C, hydrazine monohydrate, MeOH, 70 °C, 5 h, 93%; (c) PMBCl, NaH, DMF/CH_2Cl_2 (1:5), rt, 48 h, 82%; (d) 3,5-dimethyl-4-methoxyphenylmagnesium bromide, THF, 60 °C, overnight, 91%; (e) PPTS, THF/EtOH (1:1), rt, 24 h, 94%; (f) AgOTs, MeCN, rt, overnight, 99%; (g) DAST, CH_2Cl_2, 0 °C, 20 min; (h) TFA, CH_2Cl_2, 0 °C, 2 h, 61%.

mouse model injected with STZ (streptozotocin), which is toxic to the β cells in the pancreas (Figure S5). First, we measured the total fluorescence intensity of the two pancreases, and the control pancreas showed a more than 5 times higher fluorescence signal than did the STZ-treated pancreas (Figure 2D,E). Then, we prepared cryo-tissue sections based on the new protocol, and the islet imaging was successfully achieved both for control and STZ-treated islets (Figure 2F). With the simplified procedure, we could prepare hundreds of pancreatic tissue slices and took ex vivo images to compare the statistically meaningful difference between control and STZ-treated pancreases. Among 200 sections we obtained from each group, the control pancreas contained 3 times more islets than the STZ-treated pancreas (Figure 2G) and as such exhibited more than 2 times higher intensity per islet (Figure 2H). Therefore, **PiF** could be a powerful tool for the fluorescence microscopic imaging analysis of healthy β cells in the islets in various tissue sections of the disease model biopsy.

Confirmation of PiF as a Pancreatic β-Cell Probe. Next, we monitored the selective staining of **PiF** among cells within the pancreatic islets. We cultured islets after isolation according to the procedure previously reported with α-cell probe **TPα**.[21] The cultured islets were first incubated with **PiF** for 1 h, followed by **TPα** treatment for another half hour before fluorescence microscopy imaging. As expected, **TPα** was localized around the border of the pancreatic islet, where the rodent α cells are usually found, and **PiF** primarily stained the core of the islet where β cells reside (Figure 3A left). The mutually exclusive cell staining by these two dyes in the islet strongly suggested that **PiF** stained endocrine cell populations that are not α cells. To further clarify the **PiF**-stained population, we carried out immunocytochemistry with insulin antibody immediately after the addition of **PiF**. In the presence of insulin antibody, overlapping images of **PiF** (red) with anti-insulin (green) were visible (Figure 3A middle). A counterstain with glucagon antibody again demonstrated mutually exclusive cell populations between **PiF** (red) and antiglucagon (green)

https://dx.doi.org/10.1021/jacs.9b11173
J. Am. Chem. Soc. 2020, 142, 3430−3439

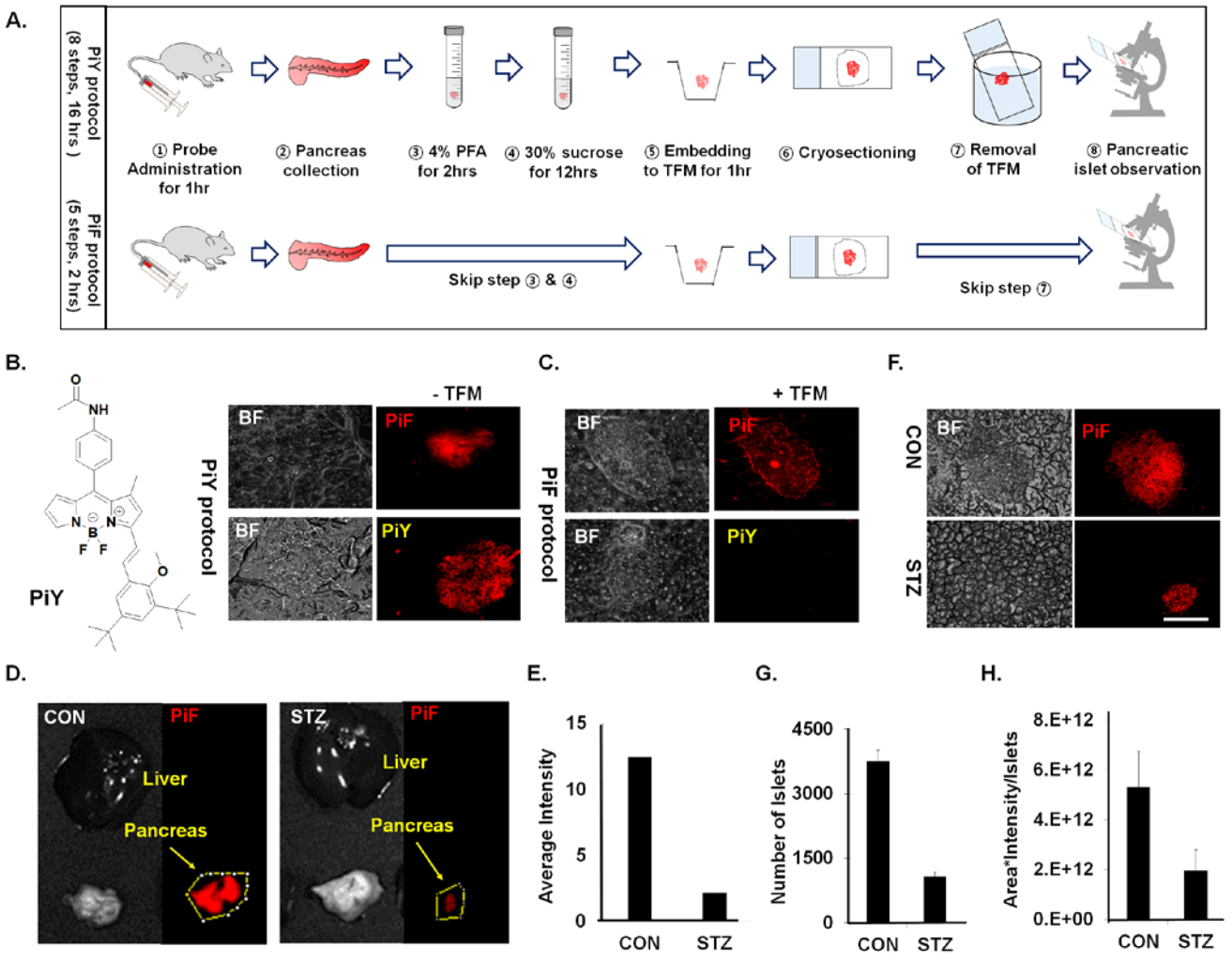

Figure 2. Facilitated procedure to visualize pancreatic islets using **PiF**. (A) Schematic procedure comparison of **PiY**- and **PiF**-detecting islets preparation and imaging. The **PiY** dissolved in 1% 4600 PEG, and 0.1% tween 20 was injected via the tail vein at 300 μM in a 250 μL quantity. The pancreas was collected after 1 h of incubation. the dissected pancreas was put into 4% PFA for 2 h and then into 30% sucrose. The pancreas was left for 12 h in the refrigerator and the next day was embedded in tissue freezing media (TFM) and kept at −80 °C for 1 h. The frozen block was cryosectioned into 20-μm-thick slices. The section after the removal of TFM was placed under the fluorescence microscope. (B) **PiY** structure and representative images of **PiY**- and **PiF**-stained islets processed with the **PiY** protocol. Both probes were visualized after the **PiY** protocol. (C) Representative images of **PiF**- and **PiY**-stained islets processed with the **PiF** protocol. Only **PiF** was visualized under the fluorescence microscope with the **PiF** protocol. The fluorescent images were taken under the TRITC filter of a Nikon Ti microscope. (D) Ex vivo fluorescent tissue images of CON and STZ mice. (Left) Untreated control mouse. (Right) STZ-streptozotocin-treated type 1 diabetic mouse. All images were taken with the IVIS Spectrum in vivo imaging system. Fluorescent images were acquired at λ_{ex} = 535 nm, λ_{em} = 585 nm. (E) Average intensity of a **PiF**-stained pancreas from CON and STZ. The region of interest in the pancreas was measured from the yellow circle. (F) Representative **PiF** stained islet section images of the control and STZ after one dropping of PBS. (G) Total number of **PiF**-stained islets from the control and STZ group (the number of control islets is 3803 vs 1116 for STZ). (H) Sum of the intensity of **PiF**-stained islets from the control and STZ group. The total number of sections collected was about 200 from each group (50 sections per mouse, n = 3, $P < 0.05$). Statistical analysis was performed under the fluorescence microscope. Scale bar: 50 μm.

(Figure 3A right). As a further confirmation, **PiF**-stained cells from isolated pancreatic islets were sorted by fluorescence-activated cell sorting (FACS), resulting in two distinct populations (Figure 3B). Ten percent of bright and dim cells were respectively collected and analyzed by real-time PCR for insulin gene expression. The insulin gene expression in **PiF** brightly stained cells was about 10 times higher as compared to that of **PiF** dimly stained cells (Figure 3C). Then, the sorted cells were also grown in 96-well plates by allowing them to attach to the bottom of the wells, and immunostaining was performed with anti-insulin and anti-glucagon antibody. Consistently, **PiF** brightly stained cells appeared positive only for insulin antibody, a hormonal marker of β cells. On the contrary, **PiF** dimly stained cells showed high positive signals for the glucagon antibody, a hormonal marker of α cells (Figure 3D). Collectively, we conclude that **PiF** is indeed a pancreatic β-cell-selective probe that can be utilized for in vivo applications. Due to the small number of islets per mouse, we decided to switch to rat islets[27] for transplantation work. Before surgery, we first evaluated the in vitro selectivity of the rat islet by **PiF** at a variety of concentrations (0, 0.25, 0.5, 1, and 2 μM) for 1 h of incubation. The rat islets were also labeled with **PiF** after PBS (phosphate-buffered saline) washing as observed under the fluorescence microscope (Figure S6A). With these islets, we measured the cell viability by CCK-8 (cell counting kit 8: live cells convert water-soluble

https://dx.doi.org/10.1021/jacs.9b11173
J. Am. Chem. Soc. 2020, 142, 3430−3439

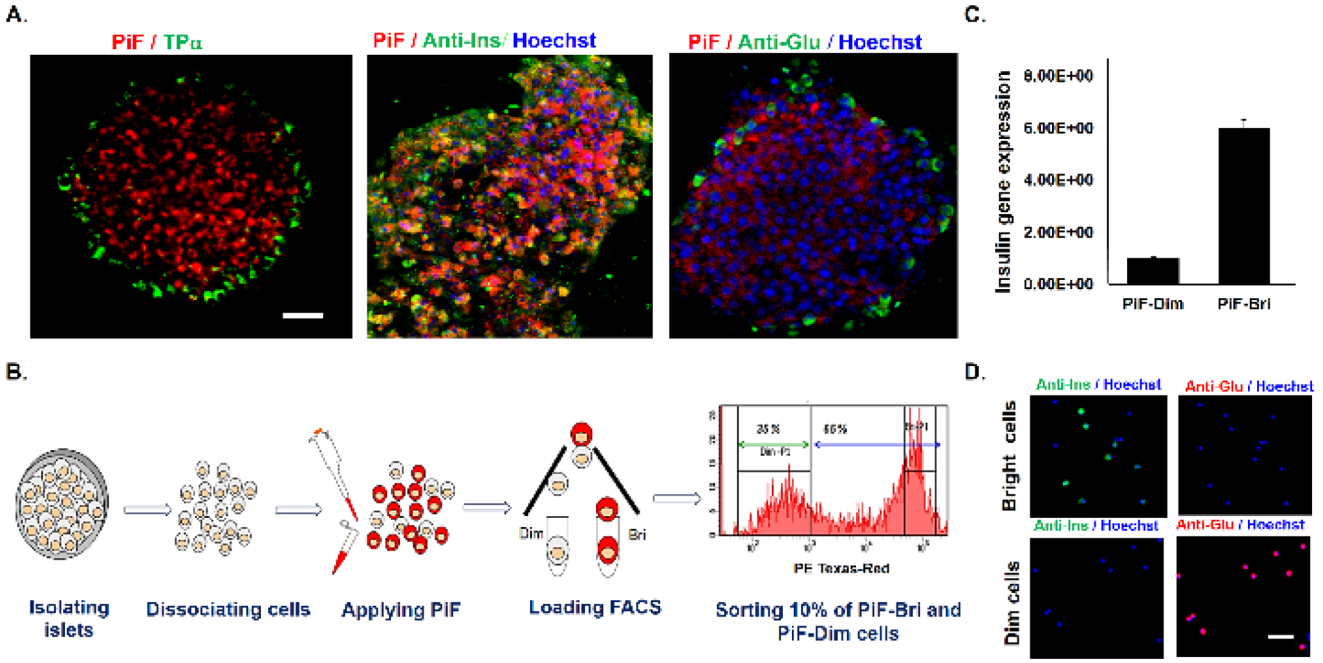

Figure 3. Confirmation of **PiF** as a pancreatic β-cell probe. (A) Fluorescent images were acquired after the cell culture of isolated islets. (Left) Merged fluorescent images of **PiF** (λ_{ex} = 535 nm, λ_{em} = 585 nm, red) and TPα (λ_{ex} = 370 nm, λ_{em} = 475 nm, green). (Middle) Merged confocal images of **PiF** (red) and anti-insulin (green: pseudocolor). Anti-insulin was imaged under a Cy5 filter. (Right) Merged confocal images of **PiF** (red) and anti-glucagon (green: pseudocolor). Anti-glucagon was imaged under a Cy5 filter. Hoechst was used for nuclei staining. (B) Scheme of the **PiF** staining process for FACS. Isolating islets from C57BL/6 mice. Dissociating islet cells. Applying **PiF** at 1 μM and incubating for 1 h. Loading **PiF**-stained cells for FACS. Isolating 10% of **PiF** bright and dim cells. (C) Real-time PCR analysis from B. The relative mRNA levels of the gene of interest are normalized to that of GAPDH. Analysis was perfomed in triplicate. (D) Immunocytochemistry (ICC) with anti-insulin and glucagon after sorting **PiF** bright and dim cells. The cells are seeded in a tissue culture dish after sorting to confirm the presence of insulin and glucagon from β cells (**PiF** bright cells) and α cells (**PiF** dim cells). All fluorescent images were taken under a Nikon Ti microscope. Scale bar: 10 μm.

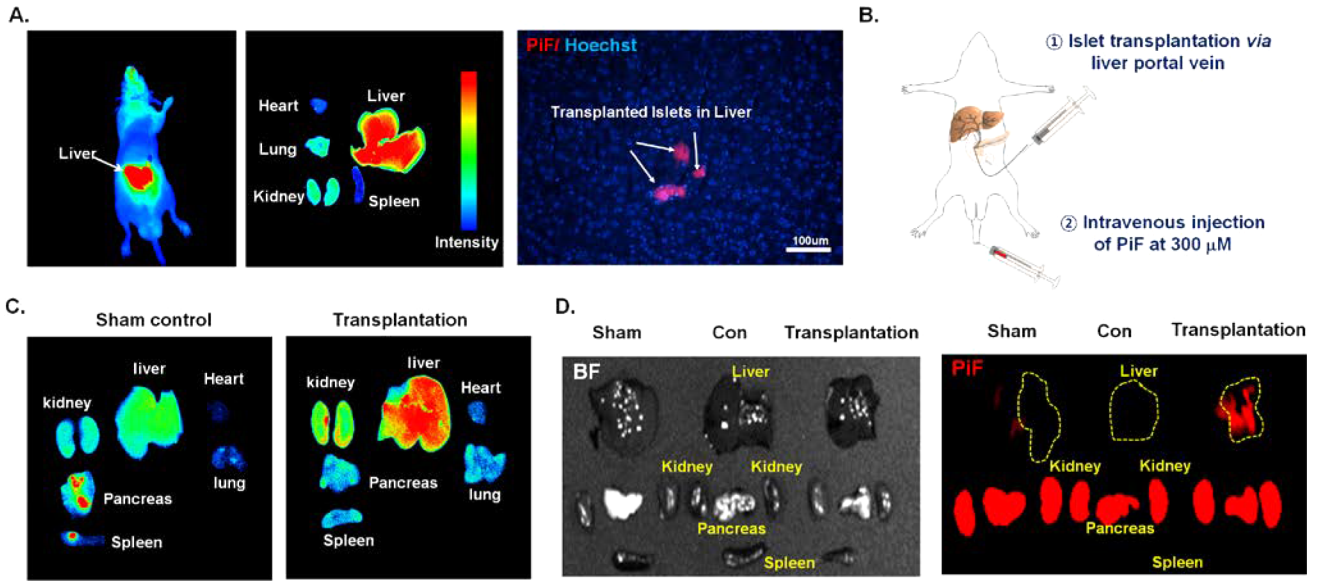

Figure 4. Transplanted rat and human islets were detected by **PiF** fluorescence imaging. (A) Rat islets (1000) labeled with **PiF** (2 μM) were intraportally transplanted to nude mice. (Left) Representative live fluorescent image 2 h after rat islet transplantation. (Middle) Ex vivo fluorescence image of a rat islet transplanted mouse. (Right) Histological evaluation of rat islet grafts in the liver. (B) Schematic illustration of imaging intrahepatic transplanted rat islets. **PiF** (300 μM, 250 μL) was intravenously injected 1 day after rat islet transplantation. (C) Ex vivo fluorescence images of sham and transplanted mice after i.v. injection of **PiF** for 1 h. The fluorescence of **PiF** was highly detected in the liver transplanted mouse against the sham control. (D) Ex vivo fluorescence images of transplanted human islets detected by **PiF**. (Left) Bright-field images (L, liver; K, kidney; P, pancreas; S, spleen). (Right) Fluorescent images from the sham, contol, and transplant. Human islets were transplanted into the liver, and 250 μL of 300 μM **PiF** was injected intravenously 1 day after transplantation (n = 3 mice from each group.)

https://dx.doi.org/10.1021/jacs.9b11173
J. Am. Chem. Soc. 2020, 142, 3430−3439

tetrazolium salt to orange formazan dye by bioreduction) assay, and **PiF** did not exhibit any significant cell toxicity on rat islets for up to 2 μM concentration as compared with untreated islets (Figure S6B). Furthermore, **PiF** showed an excellent linear correlation (R^2 = 0.97) between the fluorescence intensity and probe concentration (Figure S6C).

In Vivo Bioimaging of Transplanted Islets with the PiF Probe. **PiF**-labeled rat islets were utilized for transplantation to determine whether they can be visualized in vivo after surgery. We introduced a **PiF**-labeled rat islet graft via the liver portal vein of a nude mouse and were able to locate the **PiF** signal in the liver 2 h post-transplantation (Figure 4A left). Subsequently, we also performed ex vivo imaging of several organs (liver, heart, lung, kidney, and spleen) to confirm that the fluorescence signal came only from the liver and not from other organs (Figure 4A middle). Moreover, we performed histological analyses on the liver sections to ascertain **PiF** staining at the cellular level. As expected, we could identify **PiF**-labeled rat islets in the liver under the TRITC channel of the fluorescence microscope (Figure 4A right). To further confirm the applicability of **PiF** for in vivo imaging, we then transplanted unstained rat islets into the portal vein of a mouse followed by i.v. injection of **PiF** (300 μM, 250 μL) the following day. For surgical control, PBS was injected into the sham mouse in the portal vein instead of islets, followed by the **PiF** i.v. injection (Figure 4B). The tissues were then harvested after 2 h to image the fluorescence signal of **PiF** under ex vivo conditions. Among the various organs, the liver clearly showed a stronger intensity for **PiF** labeling in the transplanted recipient as compared to the sham control (Figure 4C). Taken together, we have demonstrated that our **PiF** small-molecule fluorescence probe is capable of visualizing rat pancreatic β cells transplanted in vivo in an ectopic site.

To then confirm that **PiF** stains human pancreatic β cells, we prepared cryo-sections of human islets after **PiF** staining. **PiF** also showed the fluorescence signal in the human islets. We then immunostained the sections using insulin antibody. From the merged images, we confirmed that the **PiF** signal is well overlapped with that of insulin antibody in the β cells of the human islets (Figure S7A). Human islets were also transplanted through the liver portal vein of the mice, and **PiF** was injected via the tail vein the day after. Ex vivo imaging revealed that the **PiF** signal was evident in the transplanted liver but not in control or sham organs (Figure 4D). The **PiF** intensity was about 2 times higher in transplanted than in the control or sham mouse (Figure S7B). Collectively, **PiF** allowed the visualization of transplanted human pancreatic β cells in the islets without antibody or genetic manipulation.

Taken together with the in vivo selectivity of **PiF** in the islet, we further carried out the stability of **PiF** via a biodistribution study for 3 h. After the intravenous administration of **PiF**, we collected organs such as plasma, white adipose, brain, heart, liver, lung, and spleen including the pancreas and measured the residual concentration of **PiF** from the tissues (Figure S8). Up to 3 h, the **PiF** still resides in the pancreas with a higher level of fluorescence intensity than in all organs except the heart (Table S1). The data showed that **PiF** is selective and stable from the pancreatic islets in vivo.

Pancreatic Islet PET Imaging with [^{18}F]PiF. Radiosynthesis of [^{18}F]**PiF** was conducted via nucleophilic aliphatic [^{18}F] fluorination from the tosylate PiT, according to our previous study[28] (see Supporting Information (SI), Experimental Procedure.) After prepurification on a tC18 Sep-Pak cartridge and purification on an HPLC, [^{18}F]**PiF** was formulated and ready to use for the animal experiment in 5% ethanol/saline solution. The measured log D value (2.19) of [^{18}F]**PiF** predicted a rapid renal excretion together with the high stability in human serum (Materials and Method). In animal studies, the tissue distribution in C57BL/6 mice was shown with comparable pancreas uptake (Table S2). The initial uptake of [^{18}F]**PiF** has shown the desirable level of 10.8 + 1.3% ID/g, and it reached the maximum level (16.1 + 5.6% ID/g) 30 min postinjection and was then washed out from the pancreas. As shown in Figure S9, the PET/CT images of [^{18}F]**PiF** visually reflected the ex vivo biodistribution of ^{18}F uptake in healthy ICR mice. [^{18}F]**PiF** possessed the highest pancreas uptake at 30 min and then was rapidly washed out (Figure 5). To confirm the specificity of [^{18}F]**PiF** in the pancreas, a blocking experiment was performed in the autoradiographic analysis (Figure S10). Blocking with excess **PiF** (100 pmol in 0.2 mL of saline) resulted in significantly reduced radioactivity uptake in the pancreas. An in vivo PET image and biodistribution analysis of [^{18}F]**PiF** in the pancreas are shown in Figure S11. The radioisotope signal intensity of [^{18}F]**PiF** at 15 min is increased dramatically, and it showed the highest peak at 30 min. After 60 min, the signal intensity is decreased by 120 min.

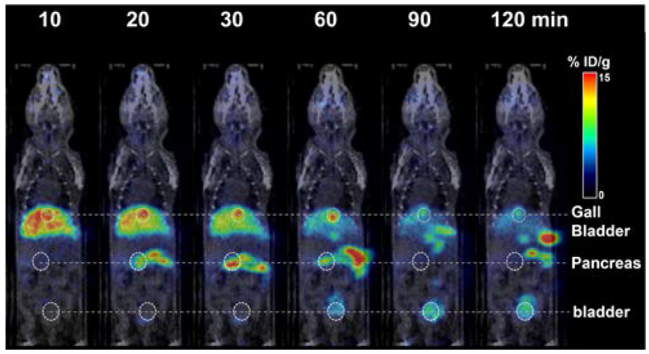

Figure 5. In vivo PET/CT images of [^{18}F]**PiF** in ICR mice. ICR mice (n = 3) were intravenously dosed with approximately 7.4 MBq of [^{18}F]**PiF**. PET acquisition in the lis mode was concomitantly started with the intravenous injection of [^{18}F]**PiF** and was performed for 120 min using a small animal PET/CT (NanoPET/CT, Mediso). The analysis was conducted using PMOD software version 3.6. Quantitative data were expressed as the percentage of the injected dose per gram of tissue (%ID/g).

DISCUSSION

Using DOFLA, we have developed a novel fluorescent probe **PiF** for pancreatic β-cell staining in rodent and human islets. Optical imaging with **PiF** allows higher resolution than MRI and PET and has broadened the application potential, especially for ex vivo tissue experiments. With **PiF**, unprecedented expeditious pancreatic islet quantitation is now possible without the requirement of antibody and also within a couple of hours instead of a conventional overnight method. **PiF** also demonstrated an excellent tissue selectivity in the pancreas with a low background compared to the liver in whole-body imaging experiments. The low liver background allowed us to transplant exogenous rat and human islets into the mouse portal vein and successfully perform an optical detection of transplanted islets. This is the first demonstration of transplanted islet detection without any prelabeling.

https://dx.doi.org/10.1021/jacs.9b11173
J. Am. Chem. Soc. 2020, 142, 3430−3439

In general, low-molecular-weight compounds have advantages for PET tracers over large protein- or peptide-based probes, including proper biodistribution and clearance profiles. Also, small molecules are less prone to elicit immunologic responses. Importantly, small molecules are more suitable for structural modifications, which are often necessary to optimize probe performance. However, in many cases, the structural modification of the probe into PET tracer could change the biological properties. We overcame this well-known problem by introducing a fluorine atom into a DOFL probe from the design stage. The fluorine atom in **PiF** could be replaced with radioactive ^{18}F for PET imaging without changing the chemical/biological property of the original **PiF**. [^{18}F]**PiF** was successfully demonstrated in pancreatic imaging in mice and can potentially be used to evaluate changes in the β-cell mass in a clinical format.[1,29] Therefore, this is the first demonstration of the systematic conversion of the fluorescence probe for β-cell imaging by combining DOFLA and fluorinated chemical motif.

CONCLUSION

We have developed a bimodal small-molecule probe which allows the visualization of rodent and, importantly, human pancreatic islets using optical and nuclear imaging techniques. As an optical imaging probe, **PiF** showed an excellent response against insulin in vitro as well as specific β-cell selectivity on the ex vivo pancreatic islet. It is noteworthy that the optimized tissue-staining protocol for **PiF** dramatically improved the procedure time by shortening the preparation time from a day to 2 h. In whole-body imaging, **PiF** showed promising staining kinetics of the pancreas through tail vein injection. The low fluorescence background signal of **PiF** in the liver allowed us to optically visualize transplanted islets on the portal vein in the liver. Finally, owing to the original design of **PiF**, the built-in fluorine atom was directly replaced with [^{18}F] to generate a chemically equivalent PET probe, and the in situ PET imaging of the pancreas was successfully demonstrated in mice.

MATERIALS AND METHODS

Synthesis of PiF. The synthesis of pancreatic β-cell probe **PiF** was summarized in Scheme 1. Known xanthone **7** was prepared from commercially available 3-fluorophenol and 4-nitrosalicylic acid according to a reported procedure.[30] The THP-protected dialkylamino group was introduced by regioselective SNAr substitution of xanthone **7**, and then nitroaryl **8** was reduced to corresponding aniline **9** by Pd catalyst/hydrazine. The aniline group was converted to N-PMB aniline using a standard protocol, and the product was treated with a Grignard reagent to provide the desired rosamine **11**. Deprotection of the THP group using PPTS in methanol provided alcohol **12**. Unfortunately, the fluorination of xanthone using DAST yielded a mixture of the desired product and inseparable alkyl chloride as a byproduct. After the counteranion exchange reaction of alcohol **12** with silver *p*-toluenesulfonate, a fluorination reaction was carried out successfully to afford the pure desired product without inseparable impurities. Finally, full deprotection of the PMB group with TFA completed the synthesis of **PiF** (Φ = 0.51, $\lambda_{ex}/\lambda_{em}$ = 535/565 nm) in seven linear steps and 14% overall yield.

In Vitro Assay of the Insulin Response. **PiF** (0.5 μM) was added to bovine insulin solution dissolved in 20 mM HEPES buffer (1% DMSO, pH 7.4) to measure the fluorescence intensity change in vitro. The concentration of insulin ranged from 0 to 400 μM. The fluorescence signal was recorded with a Spectra MaxM2 plate reader (λ_{ex} = 535 nm, λ_{em} = 565 nm). After the addition of dye, the 96-well plates were incubated for 30 min before the fluorescence intensity was read.

In Vitro Selectivity Test of PiF. In vitro selectivity assay of the insulin response. **PiF** (1 μM) was added to three different proteins (insulin, glucagon, and human serum albumin) solution dissolved in 20 mM HEPES buffer (1% DMSO, pH 7.4) to measure the fluorescence intensity change in vitro. The fluorescence was measured at 2 mg/mL for each protein. The fluorescence signal was read with a Spectra MaxM2 plate reader (λ_{ex} = 490 nm, λ_{em} = 520−670 nm). After the addition of dye, the 96-well plates were incubated for 30 min before the fluorescence intensity was read.

Preparation of PiF Injection into the Animal. **PiF** was dissolved in DMSO as a stock solution. For animal injection, **PiF** was diluted in 2% BSA in PBS solution to make a final concentration of 300 μM and 250 μL was administered through the mouse tail vein accordingly.

Pancreas Cryosection Procedure. **PiF** (250 μL, 300 μM) was injected into the mouse tail vein and incubated for 1 h. The pancreas was harvested and then put into tissue-freezing media (TFM) until frozen on the dry ice. The cryo-bock was cut into 20-μm-thick sections, and the sections covered with TFM were directly observed under a fluorescence microscope. **PiF**-stained islets with TFM were still visualized when the fluorescence was turned on. Subsequently, PBS was dropped on top of tissue to remove TFM, and **PiF**-stained islets were also confirmed. For **PiY** imaging, 4% paraformaldehyde (2 h) and 30% sucrose (overnight) were required before cryo-block preparation. The next day, the pancreas was put into a TFM medium, and the sections were obtained as in the method described above.

Fluorescence Ex Vivo Imaging. For this part of the experiment, nude mice were used. The animal was positioned at dorsal recumbences. For the transplantation animal model, pancreatic islets suspended in 0.3 mL (300 μL) of medium was injected into the hepatic portal vein. In the same manner, the sham animals received only 0.3 mL (300 μL) of medium, and the control animals did not receive any injection into the hepatic portal vein. Fluorescence imaging was done on postoperative day one. **PiF** was injected via the tail vein at a concentration of 300 μM. After 3 h of incubation, the fluorescence signal was obtained using an IVIS machine both in vivo and ex vivo. For the ex vivo imaging, organs such as liver, spleen, kidney, pancreas, and fats were included.

Diabetes Model Using Streptozotocin (STZ). STZ solution was freshly prepared in Na-citrate buffer solution and injected at 200 mg/kg as a final dosage intraperitoneally. Before STZ induction (day 0), we measured the body weight and blood glucose level after STZ injection. The blood concentration was measured with a blood glucose meter (Lifescan Inc., Milpitas, CA, USA), and STZ-treated mice had a glucose value from 15 to 40 mM. On day 10, **PiF** (300 μM, 250 μL) was injected into three each STZ and control mice. After 1 h, the pancreas was harvested to prepare the cryo-section, and pancreas sections were observed in the presence of TFM under a Nikon Ti microscope with a TRITC filter.

Statistical Analysis of Islets from CON and STZ Groups. **PiF**-stained islets were visualized to analyze statistical data by measuring the sum intensity per islet and by counting the number of islets from CON (untreated control) and STZ (streptozotocin-treated type 1 diabetic mouse group). We collected the total number of sections of about 150 from each group (50 sections per mouse, n = 3). We placed serial sections from one to three on top of the slide as labeled it as slide no. 1. To remove the same islets between slides, we made room for more than a 100 μm gap between sections. The area and intensity of **PiF**-stained islets were analyzed by NIS-Elements software provided with the Nikon Ti microscope. A value of $P < 0.05$ was considered to be statistically significant.

Cultured Islet Staining with a Fluorescence Probe. The rodent islet isolation protocol was followed as in a previously described paper. We picked up the isolated islets by hand, and the islets were incubated in 4500 mg/L D-glucose DMEM with 10% FBS and 1% penicillin-streptomycin (GIBCO) for culturing at 37 °C. The isolated islets were grown for 1 week by changing the medium every other day. **PiF** was added at 1 μM for 1 h in a new medium at 37 °C, and TPα was added to the same medium at 1 μM for 30 min before dual live islet imaging. After two-probe staining, the medium was

https://dx.doi.org/10.1021/jacs.9b11173
J. Am. Chem. Soc. 2020, 142, 3430−3439

changed to a new medium for fluorescence imaging. We took fluorescent images with a Nikon Ti microscope with TIRC for **PiF** and with FITC for TPα. Human islets were obtained from the Clinical Islet Laboratory, University of Alberta[31] Hospital, Edmonton. The use of human islets is approved by NUS Institutional Review Board (NUS-IRB) B-15-072E. Informed consent was obtained from the next of kin of the donor.

Immunostaining. After **PiF** staining on the islets, the media were changed to 4% PFA buffer, and they were incubated for 20 min and then washed with fresh PBC three times. To provide permeability, the solution was changed to 0.2% triton ×100 and incubated for 2 h and then washed again. The islet cells were transferred to a blocking buffer containing 1% bovine serum albumin as required for 1 h of incubation. Then insulin and glucagon antibodies were prepared accordingly. Guinea pig polyclonal anti-insulin (diluted 1:100, Dako) was applied for 3 h and then incubated with a Cy5-conjugated goat antiguinea pig secondary antibody (diluted 1:500, Invitrogen) for 1 h. A mouse monoclonal antiglucagon (dilution 1:500 Sigma) was used for 1 h and then placed with a Cy5-conjugated goat antimouse secondary antibody (diluted 1:1000, Invitrogen) for 1 h of incubation. These islets were observed under a Nikon A1 confocal microscope.

FACS Operation. About 150−200 islets per mouse were obtained. Dissociation media were contained with 0.2 mL of calcium and magnesium-free PBS + 0.025 mg/mL trypsin + 0.4 mg/mL EGTA + 1 mg/mL DNase. Islets were incubated for 15 min at 37 °C and subsequently were mixed by pipetting or vortex mixing for 10 s. After spinning for 5 min at 1500 rpm, the pellet was suspended in 0.5 mL of islet media in the presence of **PiF** at 1 μM. After 1 h of incubation, the dissociated cells were loaded into FACS to sort the **PiF**-Bri and **PiF**-Dim cells separately. The speared cells were utilized for real-time PCR to check the mRNA gene expression level of insulin as well as immunocytochemistry with anti-insulin and glucagon to identify **PiF** from isolated cells by images.

Quantitative Real Time PCR. Using the miRNeasy Mini Kit (QIAGEN), we isolated the total RNA as lysates from **PiF** bright and **PiF** dim cells. One-step quantitative RT-PCR was performed on a StepOne real-time PCR system using a power SYBR green RNA-to-CT 1-step kit (Applied Biosystems). The relative mRNA levels of the genes of interest were normalized to that of GAPDH. The primer sequences (5′ to 3′) are the following:

mouse INSULIN forward CCAAACCCACCCAGGCTTTTG
mouse INSULIN reverse AGTTCTCCAGCTGGTAGAGGG
mouse GAPDH forward CAAGGTCATCCATGACACTTTG
mouse GAPDH reverse GGCCATCCACAGTCTTCT GG

In Vitro Staining of Rat Pancreatic Islets with PiF. First, we dissolved Collagenase-P (1 mg/mL) (Roche, Basel, Switzerland) in HBSS (Hank's balanced salt solution) injected into the common bile duct to perform in vivo enzyme treatment and allowed the pancreas to rest for 15 min after dissection. Using Medium 199 (Sigma, St. Louis, MO, USA), the pancreas was washed two times, and then rat islets were obtained by discontinuous density gradient centrifugation combined with FicollTM Histopaque (Sigma). The purified rat islets were cultured for 1 day and subsequently treated with various concentrations of **PiF** at 0, 0.25, 0.5, 1, and up to 2 μM for 1 h. **PiF**-labeled rat islets were imaged under a fluorescence microscope (Eclipse TE2000-S; Nikon, Tokyo, Japan) after PBS washing. We also measured the correlation curve between concentration and **PiF** intensity using a microplate reader. For the cellular toxicity of **PiF**, we applied **PiF** to isolated rat islets for 1 h and then washed twice with PBS. A new islet medium (190 μL) was placed in a 96-well plate, and CCK-8 solution (10 μL) was added to incubate at 37 °C for 4 h. We measured the absorbance at 450 nm by using a microplate reader (SpectraMax M2; Molecular Devices Inc., Sunnyvale, CA).

Transplanted Rat Islet Imaging. **PiF**-labeled islets were infused as above into the portal vein using a 27-G insulin syringe (BD, Franklin Lakes, NJ, USA). Two hours after transplantation, the nude mouse was imaged in vivo using the IS4000-MM Kodak image station (Carestream Health, Rochester, NY, USA). We also transplanted 1000 unstained rat islets into nude mice intraportally. The sham animal was injected with PBS instead of islets. The next day, we injected 250 μL of 300 μM **PiF** into the tail vein of recipients. We took ex vivo images 2 h after incubation.

Human Islet Transplantation and Imaging. For this part of the experiment, we used nude mice and injected 1000 human islets. We made a ventral midline incision on the mice. Pancreatic human islets were suspended in 300 μL of human islet medium and inserted into the hepatic portal vein. The control animal underwent no surgery, and the sham animal was injected with 300 μL of only human islets (IRB reference code, NUS-IRB; reference Code, B-15-072E).

In Vivo Biodistribution Study. For the biodistribution study in a vital organ, animals were sacrificed 1 and 3 h after the administration of **PiF**. Various animal tissues such as plasma, white adipose, brain, heart, liver, lung, pancreas, and spleen were collected from each animal. Tissues were washed with saline, four volumes (w/v) of saline were added, and then the tissues were homogenized with a tissue-homogenizer (IKA Labortechnik T10 basic ULTRA-TURRAX, Staufen, Germany) at 30 000 rpm on ice. Each 200 μL of homogenate samples was extracted with 800 μL of acetronitrile containing disopyramide as an internal standard for LC-MS/MS analysis and then vortex mixed for 10 min before the extracts were centrifuged (15 000 rpm, 4 °C, 10 min). Clear supernatant was analyzed with LC-MS/MS.

LC-MS/MS Analysis. The LC-MS/MS analysis was performed on an Agilent 1200 series (Agilent Technologies, Santa Clara, CA, USA) with an Agilent 6460 LC-MS spectrometer (Agilent Technologies, USA). The chromatographic separation of **PiF** and imipramine was conducted on a hypersil gold column (50 mm × 2.1 mm, 3 μm, Thermo Scientific, USA) with a SecurityGuard C18 guard column (4 mm × 2.0 mm i.d., Phenomenex). The flow rate was 300 μL/min with a mobile phase consisting of 10 mM ammonium formate in water (eluent A) and 100% acetonitrile (eluent B) under isocratic conditions in a ratio of 20:80. The run time was 2.5 min, and the injection volume was 5 μL. Multiple reaction monitoring (MRM) mode by electrospray positive ionization (ESI) was used for the quantification of **PiF**: m/z 405.1 → 390.2 and 362 for the ionic transition. The optimized mass parameters were set as follow: gas temperature of 350 °C, sheath gas temperature of 350 °C, sheath gas flow of 11 L/min, gas flow of 10 L/min, nebulizer of 45 psi, fragmentor of 185; collision energy of 33/41, and cell accelerator voltage of 4.

PET Imaging with [^{18}F]PiF. ICR mice (n = 3) were intravenously administrated approximately 7.4 MBq of [^{18}F]**PiF**. PET acquisition in lis mode was concomitantly started with the intravenous injection of [^{18}F]**PiF** and was performed for 120 min using a small animal PET/CT. The analysis was conducted using PMOD software version 3.6. Quantitative data were expressed as the percentage of the injected dose per gram of tissue (%ID/g).

Measurement of the Lipophilicity of [18F]PiF. For the measure of lipophilicity, [**18F**]**PiF** (0.74 MBq) in 5% ethanol/saline was added to the mixture of n-octanol (5 mL) and sodium phosphate buffer (5.0 mL, 0.15 M, pH 7.4) in a test tube. After vortex mixing for 1 min, each container was then stored for 3 min at room temperature and the phases were separated. The radioactivity of samples of each phase (100 μL) was measured with a γ-counter. The lipophilicity (log D) is expressed as the logarithm of the ratio of the counts from n-octanol versus that of sodium phosphate buffer. The obtained log D of [^{18}F]**PiF** was 2.19 ± 0.03.

Measurement of the In Vitro Stability of [^{18}F]PiF in Human Serum. [^{18}F]**PiF** (3.7 MBq) in 0.4 mL of 5% ethanol/saline was mixed with an equal volume of human serum. The mixture was incubated at 37 °C for 120 min. At each time point, the sample was analyzed using a radio-TLC scanner, and the stability of the radiotracer was measeured by thin layer chromatography (10% methanol−dichloromethane, R_f = 0.3). The results showed that [^{18}F]**PiF** was stable (>99%) for up to 120 min in human serum.

https://dx.doi.org/10.1021/jacs.9b11173
J. Am. Chem. Soc. 2020, 142, 3430−3439

■ ASSOCIATED CONTENT

Supporting Information

The Supporting Information is available free of charge at https://pubs.acs.org/doi/10.1021/jacs.9b11173.

General information; experimental procedure; radiosynthesis of [^{18}F]PiF; and supplementary figures (PDF)

■ AUTHOR INFORMATION

Corresponding Authors

Dong Yun Lee − *Department of Bioengineering, College of Engineering, and BK21 PLUS Future Biopharmaceutical Human Resources Training and Research Team, and Institute of Nano Science & Technology (INST), Hanyang University, Seoul 04763, Republic of Korea;* orcid.org/0000-0001-7691-0447; Email: dongyunlee@hanyang.ac.kr

Young-Tae Chang − *Laboratory of Bioimaging Probe Development, Singapore Bioimaging Consortium, Agency for Science, Technology and Research, Singapore 138667 Singapore; Center for Self-Assembly and Complexity, Institute for Basic Science (IBS), Pohang 37673, Republic of Korea; Department of Chemistry, Pohang University of Science and Technology (POSTECH), Pohang 37673, Republic of Korea;* orcid.org/0000-0002-1927-3688; Email: ytchang@postech.ac.kr

Authors

Nam-Young Kang − *Laboratory of Bioimaging Probe Development, Singapore Bioimaging Consortium, Agency for Science, Technology and Research, Singapore 138667 Singapore; Department of Creative IT Engineering, Pohang University of Science and Technology (POSTECH), Pohang 37673, Republic of Korea*

Jung Yeol Lee − *New Drug Discovery Center, DGMIF, Daegu 41061, Republic of Korea*

Sang Hee Lee − *Department of Nuclear Medicine, Seoul National University College of Medicine, Seoul National University Bundang Hospital, Seongnam 13620, Republic of Korea; Department of Transdisciplinary Studies, Graduate School of Convergence Science and Technology, Seoul National University, Seoul 08826, Republic of Korea*

In Ho Song − *Department of Nuclear Medicine, Seoul National University College of Medicine, Seoul National University Bundang Hospital, Seongnam 13620, Republic of Korea*

Yong Hwa Hwang − *Department of Bioengineering, College of Engineering, and BK21 PLUS Future Biopharmaceutical Human Resources Training and Research Team, and Institute of Nano Science & Technology (INST), Hanyang University, Seoul 04763, Republic of Korea*

Min Jun Kim − *Department of Bioengineering, College of Engineering, and BK21 PLUS Future Biopharmaceutical Human Resources Training and Research Team, and Institute of Nano Science & Technology (INST), Hanyang University, Seoul 04763, Republic of Korea*

Wut Hmone Phue − *Laboratory of Bioimaging Probe Development, Singapore Bioimaging Consortium, Agency for Science, Technology and Research, Singapore 138667 Singapore*

Bikram Keshari Agrawalla − *Department of Chemistry, National University of Singapore, Singapore 117543 Singapore*

Si Yan Diana Wan − *Laboratory of Bioimaging Probe Development, Singapore Bioimaging Consortium, Agency for Science, Technology and Research, Singapore 138667 Singapore*

Janise Lalic − *Laboratory of Bioimaging Probe Development, Singapore Bioimaging Consortium, Agency for Science, Technology and Research, Singapore 138667 Singapore*

Sung-Jin Park − *Laboratory of Bioimaging Probe Development, Singapore Bioimaging Consortium, Agency for Science, Technology and Research, Singapore 138667 Singapore*

Jong-Jin Kim − *Center for Self-Assembly and Complexity, Institute for Basic Science (IBS), Pohang 37673, Republic of Korea*

Haw-Young Kwon − *Center for Self-Assembly and Complexity, Institute for Basic Science (IBS), Pohang 37673, Republic of Korea*

So Hee Im − *Bio &Drug Discovery Division, Korea Research Institute of Chemical Technology Yuseong-Gu, Daejeon 34114, Republic of Korea*

Myung Ae Bae − *Bio &Drug Discovery Division, Korea Research Institute of Chemical Technology Yuseong-Gu, Daejeon 34114, Republic of Korea*

Jin Hee Ahn − *Department of Chemistry, Gwangju Institute of Science and Technology (GIST), Gwangju 61005, Republic of Korea;* orcid.org/0000-0002-6957-6062

Chang Siang Lim − *Stem Cells and Diabetes Laboratory, Institute of Molecular and Cell Biology (IMCB), Agency for Science, Technology and Research (A*STAR), Singapore 138673 Singapore*

Adrian Kee Keong Teo − *Stem Cells and Diabetes Laboratory, Institute of Molecular and Cell Biology (IMCB), Agency for Science, Technology and Research (A*STAR), Singapore 138673 Singapore; Department of Biochemistry and Department of Medicine, Yong Loo Lin School of Medicine, National University of Singapore, Singapore 117597 Singapore*

Sunyou Park − *New Drug Discovery Center, DGMIF, Daegu 41061, Republic of Korea*

Sang Eun Kim − *Department of Nuclear Medicine, Seoul National University College of Medicine, Seoul National University Bundang Hospital, Seongnam 13620, Republic of Korea; Department of Transdisciplinary Studies, Graduate School of Convergence Science and Technology, Seoul National University, Seoul 08826, Republic of Korea; Center for Nanomolecular Imaging and Innovative Drug Development, Advanced Institutes of Convergence Technology, Suwon 16229, Republic of Korea*

Byung Chul Lee − *Department of Nuclear Medicine, Seoul National University College of Medicine, Seoul National University Bundang Hospital, Seongnam 13620, Republic of Korea; Center for Nanomolecular Imaging and Innovative Drug Development, Advanced Institutes of Convergence Technology, Suwon 16229, Republic of Korea;* orcid.org/0000-0002-1425-5712

Complete contact information is available at: https://pubs.acs.org/10.1021/jacs.9b11173

Author Contributions

△These authors contributed equally.

Notes

The authors declare no competing financial interest.

■ ACKNOWLEDGMENTS

This work was supported by the Institute for Basic Science (IBS, IBS-R077-A1, Korea), Agency for Science, Technology and Research (A*STAR, 15302FG148, Singapore), the Bio & Medical Technology Development Program (NRF-

2015M3A9E2030125, Korea), the Creative Materials Discovery Program (NRF-2017M3D1A1039289, Korea), the Korea Health Industry Development Institute (KHIDI; HI18C0453), and the Korea Health Technology R&D Project though KHIDI (HI19C-0316-010019).

REFERENCES

(1) Kang, N. Y.; Soetedjo, A. A. P.; Amirruddin, N. S.; Chang, Y. T.; Eriksson, O.; Teo, A. K. K. Tools for Bioimaging Pancreatic β Cells in Diabetes. *Trends Mol. Med.* **2019**, *25*, 708.

(2) Eriksson, O.; Laughlin, M.; Brom, M.; Nuutila, P.; Roden, M.; Roden, M.; Hwa, A.; Bonadonna, R.; Gotthardt, M. In vivo imaging of beta cells with radiotracers: state of the art, prospects and recommendations for development and use. *Diabetologia* **2016**, *59*, 1340.

(3) Halban, P. A.; Polonsky, K. S.; Bowden, D. W.; Hawkins, M. A.; Ling, C.; Mather, K. J.; Powers, A. C.; Rhodes, C. J.; Sussel, L.; Weir, G. G. β-cell failure in type 2 diabetes: postulated mechanisms and prospects for prevention and treatment. *J. Clin. Endocrinol. Metab.* **2014**, *99*, 1983.

(4) Gotthardt, M.; Eizirik, D. L.; Cnop, M.; Brom, M. Beta cell imaging - a key tool in optimized diabetes prevention and treatment. *Trends Endocrinol. Metab.* **2014**, *25*, 375.

(5) Meier, J. J.; Menge, B. A.; Breuer, T. G.; Müller, C. A.; Tannapfel, A.; Uhl, W.; Schmidt, W. E.; Schrader, H. Functional assessment of pancreatic beta-cell area in humans. *Diabetes* **2009**, *58*, 1595.

(6) Conget, J. I.; Sarri, Y.; González-Clemente, J. M.; Casamitjana, R.; Vives, M.; Gomis, R. Deleterious effect of dithizone-DMSO staining on insulin secretion in rat and human pancreatic islets. *Pancreas* **1994**, *9*, 157.

(7) Speier, S.; Nyqvist, D.; Cabrera, O.; Yu, J.; Molano, R. D.; Pileggi, A.; Moede, T.; Köhler, M.; Wilbertz, J.; Leibiger, B.; Ricordi, C.; Leibiger, I. B.; Caicedo, A.; Berggren, P. O. Non-invasive in vivo imaging of pancreatic islet cell biology. *Nat. Med.* **2008**, *14*, 574.

(8) Evgenov, N. V.; Medarova, Z.; Dai, G.; Bonner-Weir, S.; Moore, A. In vivo imaging of islet transplantation. *Nat. Med.* **2006**, *12*, 144.

(9) Barnett, B. P.; Arepally, A.; Karmarkar, P. V.; Qian, D.; Gilson, W. D.; Walczak, P.; Howland, V.; Lawler, L.; Lauzon, C.; Stuber, M.; Kraitchman, D. L.; Bulte, J. W. Magnetic resonance-guided, real-time targeted delivery and imaging of magnetocapsules immunoprotecting pancreatic islet cells. *Nat. Med.* **2007**, *13*, 986.

(10) Malaisse, W. J.; Damhaut, P.; Ladriere, L.; Goldman, S. Fate of 2-deoxy-2-[^{18}F]fluoro-D-glucose in hyperglycemic rats. *Int. J. Mol. Med.* **2000**, *6*, DOI: 10.3892/ijmm.6.5.549.

(11) Malaisse, W. J.; Damhaut, P.; Malaisse-Lagae, F.; Ladriere, L.; Olivares, E.; Goldman, S. J. C. Fate of 2-deoxy-2-[^{18}F]fluoro-D-glucose in control and diabetic rats. *Int. J. Mol. Med.* **2000**, DOI: 10.3892/ijmm.5.5.525.

(12) Andralojc, K.; Srinivas, M.; Brom, M.; Joosten, L.; de Vries, I. J.; Eizirik, D. L.; Boerman, O. C.; Meda, P.; Gotthardt, M. Obstacles on the way to the clinical visualisation of beta cells: looking for the Aeneas of molecular imaging to navigate between Scylla and Charybdis. *Diabetologia* **2012**, *55*, 1247.

(13) Blomberg, B. A.; Codreanu, I.; Cheng, G.; Werner, T. J.; Alavi, A. Beta-cell imaging: call for evidence-based and scientific approach. *Mol. Imaging. Biol.* **2013**, *15*, 123.

(14) Harris, P. E.; Leibel, R. L. Neurofunctional imaging of beta-cell dynamics. *Diabetes, Obes. Metab.* **2012**, *14*, 91.

(15) Botsikas, D.; Terraz, S.; Vinet, L.; Lamprianou, S.; Becker, C. D.; Bosco, D.; Meda, P.; Montet, X. Pancreatic magnetic resonance imaging after manganese injection distinguishes type 2 diabetic and normoglycemic patients. *Islets.* **2012**, *4*, 243.

(16) Goland, R.; Freeby, M.; Parsey, R.; Saisho, Y.; Kumar, D.; Simpson, N.; Hirsch, J.; Prince, M.; Maffei, A.; Mann, J. J.; Butler, P. C.; Van; Heertum, R.; Leibel, R. L.; Ichise, M.; Harris, P. E. ^{11}C-dihydrotetrabenazine PET of the pancreas in subjects with long-standing type 1 diabetes and in healthy controls. *J. Nucl. Med.* **2009**, *50*, 382.

(17) Normandin, M. D.; Petersen, K. F.; Ding, Y. S.; Lin, S. F.; Naik, S.; Fowles, K.; Skovronsky, D. M.; Herold, K. C.; McCarthy, T. J.; Calle, R. A.; Carson, R. E.; Treadway, J. L.; Cline, G. W. In vivo imaging of endogenous pancreatic beta-cell mass in healthy and type 1 diabetic subjects using ^{18}F-fluoropropyl-dihydrotetrabenazine and PET. *J. Nucl. Med.* **2012**, *53*, 908.

(18) Minn, H.; Kauhanen, S.; Seppänen, M.; Nuutila, P. ^{18}F-FDOPA: a multiple-target molecule. *J. Nucl. Med.* **2009**, *50*, 1915.

(19) Luo, Y.; Pan, Q.; Yao, S.; Yu, M.; Wu, W.; Xue, H.; Kiesewetter, D. O.; Zhu, Z.; Li, F.; Zhao, Y.; Chen, X. Glucagon-Like Peptide-1 Receptor PET/CT with ^{68}Ga-NOTA-Exendin-4 for Detecting Localized Insulinoma: A Prospective Cohort Study. *J. Nucl. Med.* **2016**, *57*, 715.

(20) Wei, W.; Ehlerding, E. B.; Lan, X.; Luo, Q. Y.; Cai, W. Molecular imaging of β-cells: diabetes and beyond. *Adv. Drug Delivery Rev.* **2019**, *139*, 16.

(21) Agrawalla, B. K.; Chandran, Y.; Phue, W. H.; Lee, S. C.; Jeong, Y. M.; Wan, S. Y.; Kang, N. Y.; Chang, Y. T. Glucagon-Secreting Alpha Cell Selective Two-Photon Fluorescent Probe TP-α: For Live Pancreatic Islet Imaging. *J. Am. Chem. Soc.* **2015**, *137*, 5355.

(22) Kang, N. Y.; Lee, S. C.; Park, S. J.; Ha, H. H.; Yun, S. W.; Kostromina, E.; Gustavsson, N.; Ali, Y.; Chandran, Y.; Chun, H. S.; Bae, M.; Ahn, J. H.; Han, W.; Radda, G. K.; Chang, Y. T. Visualization and isolation of Langerhans islets by a fluorescent probe PiY. *Angew. Chem., Int. Ed.* **2013**, *52*, 8557.

(23) Vendrell, M.; Zhai, D.; Er, J. C.; Chang, Y. T. Combinatorial strategies in fluorescent probe development. *Chem. Rev.* **2012**, *112*, 4391.

(24) Kang, N. Y.; Ha, H. H.; Yun, S. W.; Yu, Y. H.; Chang, Y. T. Diversity-driven chemical probe development for biomolecules: beyond hypothesis-driven approach. *Chem. Soc. Rev.* **2011**, *40*, 3613.

(25) Yun, S. W.; Kang, N. Y.; Park, S. J.; Ha, H. H.; Kim, Y. K.; Lee, J. S.; Chang, Y. T. Diversity oriented fluorescence library approach (DOFLA) for live cell imaging probe development. *Acc. Chem. Res.* **2014**, *47*, 1277.

(26) Ahn, Y. H.; Lee, J. S.; Chang, Y. T. Combinatorial rosamine library and application to in vivo glutathione probe. *J. Am. Chem. Soc.* **2007**, *129*, 4510.

(27) Carter, J. D.; Dula, S. B.; Corbin, K. L.; Wu, R.; Nunemaker, C. S. A practical guide to rodent islet isolation and assessment. *Biol. Proced. Online* **2009**, *11*, 3.

(28) Perrone, M.; Moon, B. S.; Park, H. S.; Laquintana, V.; Jung, J. H.; Cutrignelli, A.; Lopedota, A.; Franco, M.; Kim, S. E.; Lee, B. C.; Denora, N. A Novel PET Imaging Probe for the Detection and Monitoring of Translocator Protein 18 kDa Expression in Pathological Disorders. *Sci. Rep.* **2016**, *6*, 20422.

(29) Haldorsen, I. S.; Ræder, H.; Vesterhus, M.; Molven, A.; Njølstad, P. R. The role of pancreatic imaging in monogenic diabetes mellitus. *Nat. Rev. Endocrinol.* **2012**, *8*, 148.

(30) Yun, S. W.; Leong, C.; Bi, X.; Ha, H. H.; Yu, Y. H.; Tan, Y. L.; Narayanan, G.; Sankaran, S.; Kim, J. Y.; Hariharan, S.; Ahmed, S.; Chang, Y. T. A fluorescent probe for imaging symmetric and asymmetric cell division in neurosphere formation. *Chem. Commun.* **2014**, *50*, 7492.

(31) Teo, A. K. K.; Lim, C. S.; Cheow, L. F.; Kin, T.; Shapiro, J. A.; Kang, N. Y.; Burkholder, W.; Lau, H. H. Single-cell analyses of human islet cells reveal de-differentiation signatures. *Cell. Death. Discovery* **2018**, *4*, 14.

https://dx.doi.org/10.1021/jacs.9b11173
J. Am. Chem. Soc. 2020, 142, 3430−3439